

Effects of Confinement on Molecular Motor-Driven Self-Assembly of Ring Structures

HAIQING LIU¹ and GEORGE D. BACHAND²

¹Nanoscale Science Department, Sandia National Laboratories, Albuquerque, NM 87185, USA; and ²Nanosystems Synthesis and Analysis Department, Center for Integrated Nanotechnologies, Sandia National Laboratories, PO Box 5800, MS 1303, Albuquerque, NM 87185, USA

(Received 16 August 2012; accepted 24 October 2012; published online 7 November 2012)

Associate Editor Jung-Chi Liao & Henry Hess oversaw the review of this article.

Abstract—Active transport by kinesin molecular motors has been used to assemble ring nanocomposites comprised of biotinylated microtubules and streptavidin-coated quantum dots. Here we studied the effects of two-dimensional surface confinement on ring self-assembly using substrates of microfluidic channels or periodic post arrays. Microfabricated devices were composed of gold–silicon oxide surfaces where the gold surfaces were functionalized with thiol-based self-assembled monolayers, which enabled selective adsorption of kinesin to silicon surfaces. Confinement of ring self-assembly within microfluidic channels was observed as a change in the distribution of ring diameters, specifically by placing an upper limit on the diameter capable of forming in the channels. Confining assembly using periodic post arrays where the edge-to-edge spacing was 2 μm resulted in a significantly smaller average diameter when compared against those formed in arrays with 5 and 10 μm spacing. Differences in diameters formed in 5 and 10 μm arrays were not observed. Observations of ring composite assembly along channel edges on the top surface, as well as around posts in the arrays confirm the fundamental role of active transport-induced mechanical strain in initiating the self-assembly process.

Keywords—Molecular assembly, Kinesin, Self-organization, Molecular crowding, Confinement.

INTRODUCTION

The critical importance of self-assembly and organization in biological systems has been widely recognized, and has served as a motivation for materials chemists and engineers.^{35,39,40} Large, structurally complex self-assembled artificial materials are, however,

infrequently encountered due to limitations associated with diffusion and chemical equilibria. Active transport of macromolecular building blocks by biomolecular motors has been proposed as a means to circumvent these problems through reliance on facilitated transport in place of diffusive mechanisms.¹¹ In addition, the conversion of chemical energy into mechanical work enables biomolecular motors to exert forces considerably larger than thermal forces that may, in turn, be used to assemble a variety of non-equilibrium structures.^{8,23,26}

A simple model system for biomolecular motor-driven self-assembly involves the formation of ring nanocomposites comprised of biotinylated microtubules and streptavidin-coated quantum dots (QDs) based on active transport by surface-adsorbed kinesin motors.^{2,23,24} Here, biotinylated microtubules (25 nm diameters, several microns long) serve as a tubular scaffold for adsorbing a variety of streptavidin-functionalized cargoes.^{1–3,27} If streptavidin-QDs are mixed with biotinylated microtubules in bulk solution, and in the absence of kinesin motors, randomly organized, three-dimensional aggregates emerge as the primary structural morphology.¹ Introduction of streptavidin-QDs to biotinylated microtubules bound to and moving across kinesin-coated surfaces generates distinctly different morphologies including ring-structured nanocomposites.^{2,23,24} Assembly of such non-equilibrium materials demonstrates how active transport may be applied to assemble structures that cannot be formed through traditional self-assembly routes.

In addition to streptavidin-coated nanoparticles, kinesin-driven assembly of microtubule ring structures (e.g., spools) has been achieved using streptavidin alone.^{8,12,19–21,26} While the morphologies are similar, the assembly and behavior of the ring structures formed with just streptavidin differ from those formed with streptavidin-QDs. For example, streptavidin-rings are

Address correspondence to George D. Bachand, Nanosystems Synthesis and Analysis Department, Center for Integrated Nanotechnologies, Sandia National Laboratories, PO Box 5800, MS 1303, Albuquerque, NM 87185, USA. Electronic mail: gdbacha@sandia.gov

able to “unspool” by the unzipping of biotin-streptavidin bonds,¹² whereas such phenomena have not been observed for streptavidin-QD ring structures. In both cases, the ring structures formed by motor-driven self-assembly are capable of storing considerable energy (i.e., thousands of kT), and require the dissipation of energy through hydrolysis of ATP to bend the rigid microtubules^{9,30} into the ring morphologies.^{23,24} Based on central role of energy dissipation, manipulation of the active transport should enable additional control over the self-assembly process and potentially generate structures with different physical properties.

Directional control over kinesin-based active transport has been achieved using a number of methods including microfabricated channels,^{4–6,13–15,28,29,37} magnetic fields,^{16,17} and electric fields.^{18,22,38} Of these methods, microtubule transport on microfabricated substrates, combined with surface functionalization, is an attractive approach for studying how ring composite self-assembly may be affected by confinement of microtubule transport. Self-assembly of biological and synthetic materials in confined geometries and spaces has become of interest in recent years based on the unique behaviors and phenomena that emerge in confined systems.³³ Self-organization of microtubule structures, for example, in lipid vesicles is strongly dependent on the bending stiffness of the membrane.³² The objective of our work was to characterize the effects of microscale confinement on the kinesin-driven assembly of ring nanocomposites. We hypothesized that localization of kinesin attachment and physical confinement of microtubule transport would provide a means of controlling the overall size and shape of self-assembled ring composites.

EXPERIMENTAL METHODS

Preparation of Microtubules and Motor Proteins

Unlabeled, biotinylated, and rhodamine-labeled tubulin were purchased from Cytoskeleton, Inc. (Denver, CO). Fluorescent, biotinylated microtubules were prepared by rehydrating lyophilized tubulin in BRB80 buffer (80 mM PIPES pH 6.9, 1 mM $MgCl_2$, 1 mM EGTA) containing 1 mM GTP and 10% glycerol (5 mg/mL final tubulin concentration), and polymerizing at 37 °C for 20–25 min. The polymerized microtubules were then stabilized by diluting 100-fold into BRB80T (BRB80 with 10 μM paclitaxel).

The *Drosophila melanogaster* kinesin-1 motor protein was used to bind and transport microtubules along the gold-SiO₂ substrates containing the microfluidic channels or post arrays. The histidine-tagged kinesin heavy chain motor was prepared by expressing the pPK113 plasmid⁷ in *Escherichia coli* BL21 (DE3)

pLysS. When the culture reached an OD_{600 nm} of ~0.7, protein expression was induced by addition of isopropylthio- β -galactoside (IPTG) to final concentration of 0.5 mM. Cells were harvested by centrifugation at 9000 $\times g$, and stored at –80 °C until used. Cells were lysed using BugBuster[®] with Benzonase[®] (EMD BioSciences, Inc., Billerica, MA) and AEBSF (4-(2-Aminoethyl) benzenesulfonyl fluoride hydrochloride; Sigma-Aldrich Inc., St. Louis, MO), and kinesin was purified on a Ni-NTA column as previously described.^{1,7}

Substrate Fabrication

The effects of physical confinement were evaluated using two patterned surfaces: (1) 5 and 10 μm wide microfluidic channels (300 nm depth), and (2) microscale post arrays (500 nm tall). For the latter, the posts were fabricated with diameters of 2, 5, and 10 μm , and were periodically spaced on a square lattice with edge-to-edge distances of 2, 5, or 10 μm . Substrates for fabrication were 500- μm -thick silicon wafers with 1- μm -thick layer of SiO₂ thermally grown on top, which were prebaked at 120 °C for 2 min to remove moisture. High-resolution positive resist 950 polymethylmethacrylate (PMMA) C9 (Microchem Corp., Newton, MA) was spin-coated onto the wafers at 2500 rpm for 45 s yielding a 2.2- μm thick layer, followed by a 30-min pre-exposure bake at 170 °C. The channel and post structures were defined by chrome quartz mask using deep UV (248 nm) of an OAI contact aligner, with a dose of 900 mJ/cm². A developing solution consisting of 1:1 methyl-isobutyl ketone (MIBK) and isopropyl alcohol (IPA) was allowed to react for 2 min, followed by a 30 s immersion in IPA to stop the development. Patterned substrates were then dried with nitrogen, and an oxygen plasma (5 W, 60 s) was used to descum the surfaces. Directional e-beam evaporation was then used to deposit a 10-nm-thick titanium adhesion layer and a subsequent 500-nm gold layer onto the patterned substrates. Lift-off (i.e., removal of the metal layers from the channels or interstitial space in the post arrays) was performed by sonicating the samples in acetone bath followed by rinse in fresh acetone and IPA with the use of air brush.

Substrate Functionalization—Alkanethiol Monolayers Deposition

Functionalization of patterned substrates with thiol self-assembled monolayers (SAMs) was used to selectively localize kinesin motor proteins to SiO₂ surface (i.e., bottom of channels and interstitial space in the post arrays). The terminal sulfur group of the alkanethiols adsorbs to the gold posts and channel tops and

sidewalls, forming SAMs with specific chemical functionality. Substrates were first cleaned with acetone (air brush) and IPA, followed by a combination of oxygen plasma and wet cleaning. Oxygen plasma (250 W, 100 °C) was performed for 10 min to remove the fatty films on surface; ddH₂O was used to rinse the substrate thoroughly to remove all the free particles embedded in the organics. Oxygen plasma was used again to make the substrate surface hydrophilic and ready for SAM deposition. Gold-SiO₂ substrates were immediately transferred into the thiol SAM solution and incubated for 12 h. The substrates were subsequently rinsed with ethanol and dried with nitrogen. Functionalized substrates were used immediately for motility-based experiments.

Four different SAMs were used to evaluate the role of surface chemistry on kinesin adsorption and self-assembly of ring nanocomposites in the microfluidic channels. Two PEG-based SAMs (EG₄-thiol:(11-mercapto-undecyl)tetra(ethylene glycol) and EG₆-thiol:(11-mercapto-undecyl)hexa(ethylene glycol; Sigma-Aldrich Inc., St. Louis, MO) that are known to resist protein adsorption^{25,31} were used to render the gold surfaces as “anti-fouling.” Gold surfaces on the channel substrates were also functionalized with SAMs anionic (12-mercapto-dodecanoic acid; Sigma-Aldrich Inc., St. Louis, MO) and cationic (11-mercapto-undecyl)-*N,N,N*-trimethylammonium bromide; Sigma-Aldrich Inc., St. Louis, MO) terminal groups to evaluate potential electrostatic effects on self-assembly. For post array patterns, only PEG₄-thiol SAMs were used to functionalize the gold surface based on the experimental results obtained with the channel patterns.

Ring Self-Assembly on Micropatterned Surfaces

Gliding motility assays and ring self-assembly were performed as previously described.^{23,24} Briefly, all buffers were added to device chips by drop casting, followed by incubation in a moisture-controlled environment. Fluid was exchanged by removing the previous droplet and flushing with the next component twice before incubation. Substrates were first treated with a casein solution in BRB80 (0.5 mg/mL) for 10 min, washed, and incubated with a kinesin solution in BRB80 (5 μg/mL kinesin, 0.2 mg/mL casein, 1 mM ATP) for 10 min. Microtubules were diluted to a filament density of $3 \times 10^4/\mu\text{m}^2$ in motility solution of BRB80 supplemented with 10 μM paclitaxel, 1 mM ATP, 0.1 mg/mL casein, and an anti-fade cocktail (0.2 mM glucose, 0.2 mg/mL glucose-oxidase, 0.08 mg/mL catalase and 2% β-mercaptoethanol). Microtubules were incubated for 10 min on substrates to allow attachment to kinesin-coated surfaces, followed by a rinse with motility solution to remove free

floating microtubules. Lastly, a solution of QD[®]525 Streptavidin conjugates (Life Technologies, Grand Island, NY) was diluted in motility solution to a concentration of 1 nM, and then added to the substrates. A 170-μm thick microscope cover slip was placed on top of device chip after completion of all steps to allowed observation under inverted fluorescence microscopy (Olympus IX71) using a 100× oil-immersion objective (Olympus, N.A. = 1.40). A Hamamatsu C7780 color CCD-camera was used to collect images. Ring self-assembly was also visualized using a FEI Nova NanoLab 600 field emission scanning electron microscope (SEM) where the sample was sputter coated with 200-Å layer of gold and imaged with 5 keV using Through the Lens Detector (TLD).

RESULTS

Ring Self-Assembly in Channels—Surface Chemistry Effects

Microfluidic channels were fabricated by depositing and patterning gold on a silicon wafer, enabling the use of thiol SAMs to chemically functionalize the top and side-walls of the channels (Fig. 1). To understand the role of surface chemistry on ring assembly, gold surfaces were functionalized with SAMs to generate anionic, cationic, or anti-fouling PEG surfaces. Rings assembled on the bottom of the channels regardless of the SAM chemistry (Fig. 2), which confirmed the adhesion and function of kinesin motors on SiO₂ surfaces. For gold surfaces, motor-driven assembly of rings was not observed on the top surfaces of channel patterns functionalized with cationic and anti-fouling SAMs (Figs. 2b–2d). In these cases the combination of surface chemistry and topographic patterning enables the selective adsorption of kinesin to SiO₂ surfaces, and subsequently localizes assembly of ring composites only within the confines of the microfabricated channels. In contrast, motor-driven assembly of rings was observed on gold surfaces functionalized with anionic SAMs (Fig. 2a), suggesting that kinesin motors can adsorb equally to both the SiO₂ and anionic SAMs. Ring composites were often assembled along the top edge of the channels functionalized with anionic SAMs, and, in several cases, were observed to extend past the channel edge (Fig. 3a). In these cases, part of the ring was bound by motors attached to the gold-SAM surfaces, while the other part was unattached to any surface. These rings also maintained the ability to rotate despite being only partially attached to a surface. Interestingly, ring composites also detached from the anionic surfaces over time and could be observed floating in solution for >2 h post-detachment (Fig. 3b). Approximately 10–20% of total ring

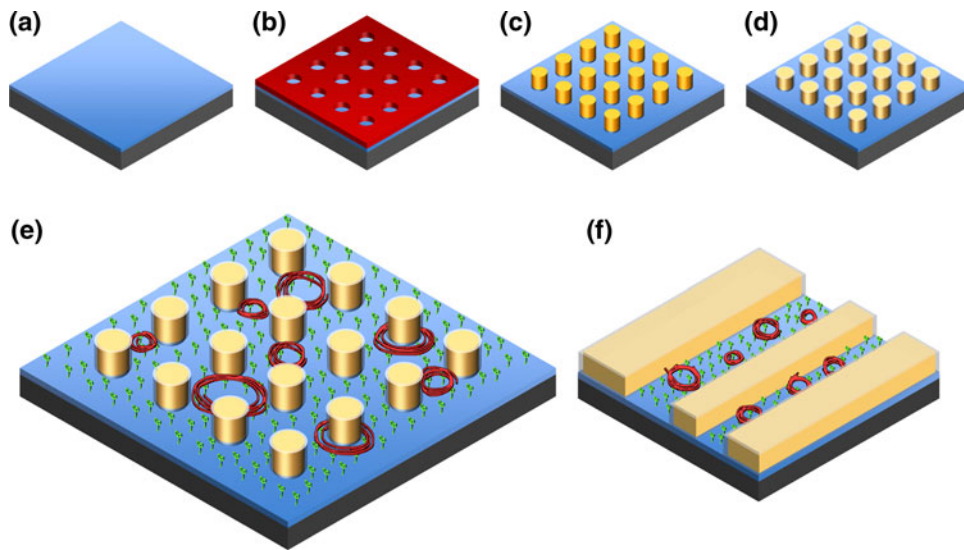


FIGURE 1. Fabrication process. (a) Substrates were 500- μm -thick silicon wafers with 1- μm -thick layer of SiO_2 thermally grown on top. (b) High resolution positive resist PMMA was spin-coated onto the substrates, and photolithography was used to define the post or channel structures. (c) Lift-off procedure was done to remove the resist with metal layers around the posts; gold posts or channels with a titanium adhesion layer were constructed. (d) SAMs was deposited on gold surfaces as an anti-fouling approach for blocking of kinesin adsorption. Microtubules assembled into ring composite structures on kinesin-coated SiO_2 surface, where the self-assembly confined by the posts (e) or channels walls (f).

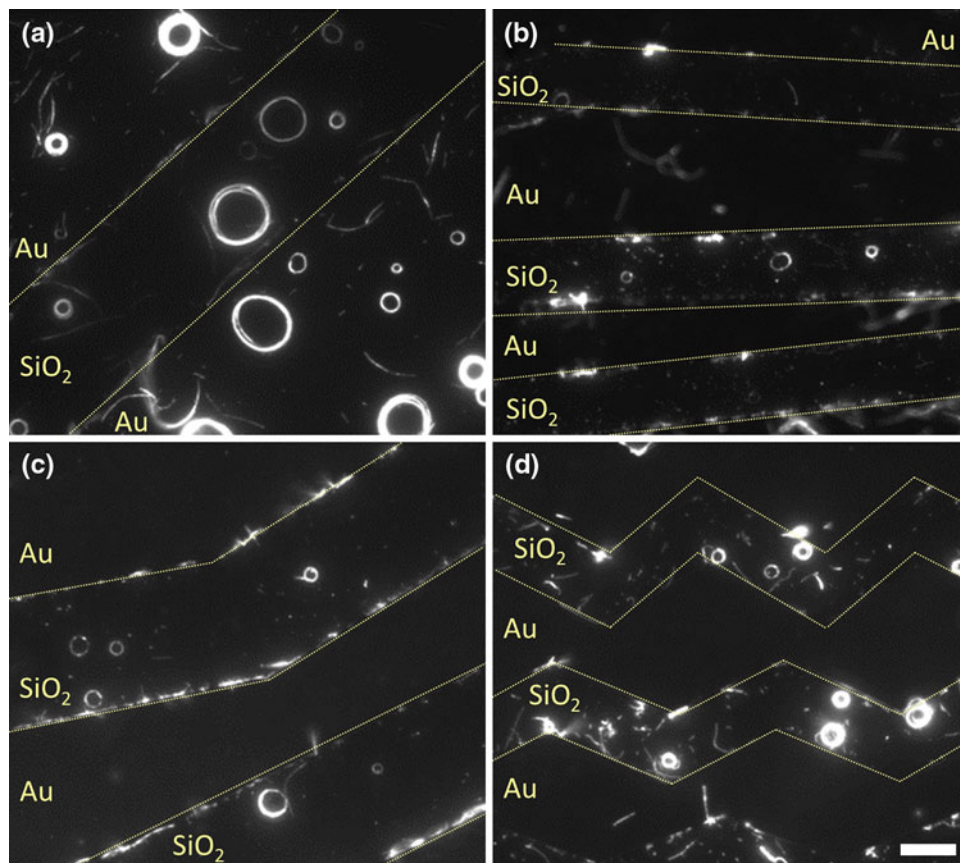


FIGURE 2. Formation of ring composites on gold- SiO_2 patterns where the gold was functionalized with (a) anionic, (b) cationic, or antifouling (c) EG4 and (d) EG6 SAMs. Dotted lines were added to emphasize the channel edges. Scale bar = 5 μm .

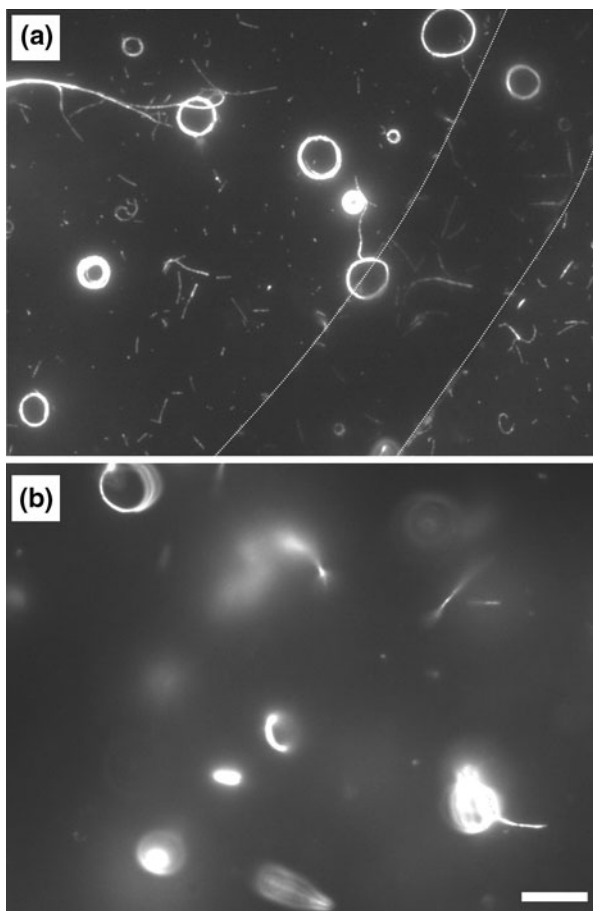


FIGURE 3. (a) Assembly of ring composites on SiO₂ and gold surfaces functionalized with anionic SAMs. Dotted lines were added to emphasize the channel edges. Here an example of a ring assembled on the top surface (gold) of the channel and protruding over the top edge. (b) Fluorescence photomicrograph of motor-assembled rings that detached from anionic SAM-functionalized surfaces and persisted in solution. Scale bars = 5 μm.

population detached from the SAM-coated surfaces, whereas ring detachment was not observed from SiO₂ surfaces.

Ring Self-Assembly in Channels—Topographic Effects

Effects on confinement of self-assembly in micro-scale channels was evaluated using patterned substrates functionalized with the EG4 SAM based on its anti-fouling behavior (Fig. 2c). The inner diameter of fifty rings assembled in 5 μm channels varied from 0.8 to 5.3 μm with an average of 2.1 ± 1.1 μm (± SD), whereas the inner diameter of fifty rings formed in the 10 μm channels varied from 0.9 to 12.1 μm with an average of 2.6 ± 2.0 μm. For both channel sizes, the inner diameters displayed a Gaussian distribution (*not shown*), including values that exceeded the channel width. Here the rings adopted an ovular shape in the

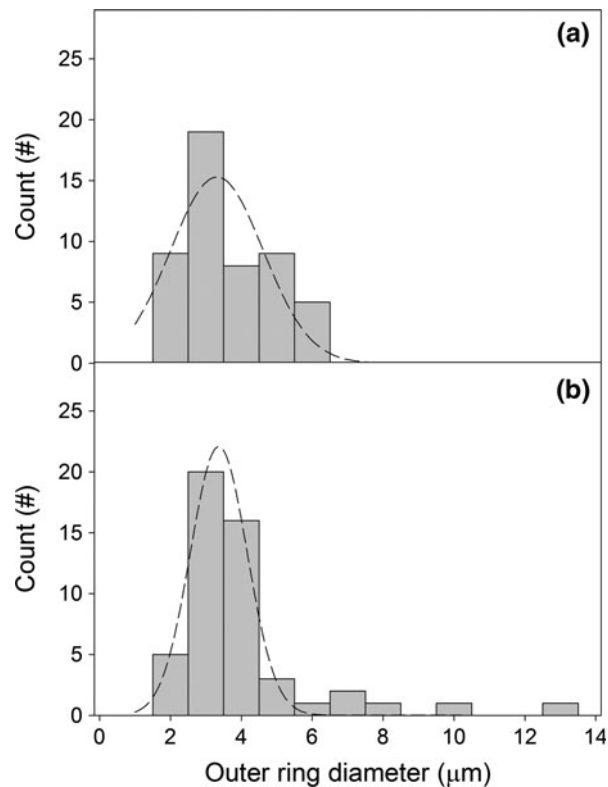


FIGURE 4. Histogram of the outer diameters of ring nano-composites assembled in (a) 5 or (b) 10 μm wide channels. Distributions were fit by nonlinear regression with a Gaussian peak equation, $y = a * e^{(-0.5 * ((x - x_0) / b)^2)}$. Coefficients of determination (R^2) for the 5 or 10 μm channels were 0.83 and 0.98, respectively.

channel where the minor axis length is confined by the channel width. Overall, no significant difference was observed between the mean inner diameters of the ring formed in the different sized channels ($p = 0.141$). The outer diameters of rings assembled in 5 μm channels varied from 2.0 to 6.1 μm with an average of 3.6 ± 1.2 μm ($N = 50$). In contrast, the outer diameter of the rings formed in the 10 μm channels, the outer ring diameter varied from 2.3 to 13.4 μm with an average of 4.1 ± 2.0 μm ($N = 50$). As with the inner diameter, observed ring diameters exceeded the width of the channels in cases where the rings adopted an ovular shape in the channel. Significant difference were not observed between the mean outer diameters of the ring formed in the different sized channels ($p = 0.376$). The outer diameters also displayed Gaussian distributions (Fig. 4); the coefficient of determination (R^2), however, for the 5 μm (0.83) was smaller than that for the 10 μm channels (0.98), suggesting that these data are less stochastically distributed. Further examination of the outer diameter distributions reveals how confinement in channels affects ring self-assembly. Specifically, comparing the upper tails of the two

distributions, ring diameters greater than $6 \mu\text{m}$ were not observed for the $5 \mu\text{m}$ channels (Fig. 4). Thus, confinement of ring self-assembly in channels can limit the maximum achievable ring diameter, despite having a minimal effect on the average diameter of a population of rings.

Ring Self-Assembly in Post Arrays

The diameter and edge-to-edge spacing of posts in a square array were varied to provide a size-range of interstitial space in which ring self-assembly could occur. The maximum ring diameter capable of forming in a square array pattern can be estimated by:

$$D_{\text{Max}} = \sqrt{2(2r + p)^2 - 2r} \quad (1)$$

where r is the radius of the post, and p is the edge-to-edge distance between the posts. Based on these parameters, the maximum predicted outer ring diameter capable of forming in the square array interstitial space covered a range from 3.7 to $18.3 \mu\text{m}$ (Table 1). Measured ring diameters ($N = 180$) in these arrays were analyzed by Two-way Analysis of Variance (ANOVA) to assess the main effects (i.e., post diameter and edge-to-edge spacing) and the interaction term (i.e., diameter \times spacing). Only the edge-to-edge spacing significantly impacted the diameter of rings self-assembled in the square arrays ($p < 0.001$; Fig. 5). Specifically, the mean outer diameter of rings assembled in patterns with $2 \mu\text{m}$ edge-to-edge spacing ($3.1 \pm 0.2 \mu\text{m}$) was significantly smaller than those formed in patterns with either the 5 or $10 \mu\text{m}$ spacing (4.6 ± 0.2 and $4.7 \pm 0.2 \mu\text{m}$, respectively; $p < 0.001$). No difference in diameters was observed for rings assembled in patterns with the 5 and $10 \mu\text{m}$ spacing ($p = 0.104$). Similarly significant differences in the mean outer ring diameter were also not observed based

TABLE 1. Maximum predicted ring diameter and percentage of available surface area of kinesin adhesion in square post array patterns with varying the diameter and edge-to-edge spacing.

Post diameter (μm)	Edge-to-edge spacing (μm)	Maximum predicted diameter (μm)	Percentage of surface area for kinesin adhesion (%)
2	2	3.7	80
2	5	7.9	94
2	10	15.0	98
5	2	4.9	60
5	5	9.1	80
5	10	16.2	91
10	2	7.0	45
10	5	11.2	65
10	10	18.3	80

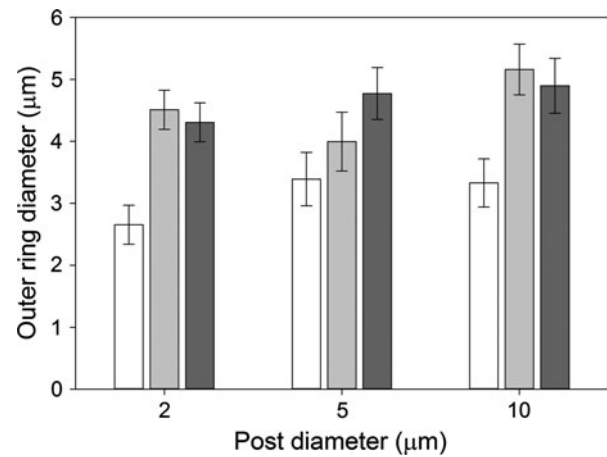


FIGURE 5. Outer ring diameter self-assembled in square arrays of posts with diameters of 2, 5, and $10 \mu\text{m}$ and edge-to-edge spacing distances of 2 (white bar), 5 (light gray bar), and 10 (dark gray bar) μm . Error bars = standard error of the mean.

on post diameter ($p > 0.08$). Because the area of the interstitial space is defined by both the post diameter and the spacing, it was expected that the interaction term would have significantly affect the ring diameter. However, no differences in the mean ring diameter were observed based on the interaction between post diameters and spacing used in these experiments ($p > 0.05$).

Qualitative differences in ring self-assembly based on both post diameter and edge-to-edge spacing were noted in both fluorescence and SEM imaging (Figs. 6, 7). In all patterns, oligomeric bundles of microtubules in addition to ring composites were observed in the interstitial spaces, as well as moving through the post patterns (Fig. 6). However, fewer ring composites were observed in patterns with $2 \mu\text{m}$ edge-to-edge spacing, particularly with $10 \mu\text{m}$ posts, due to the limited available surface area for microtubule attachment to kinesin (Table 1). As with the channel patterns, ring composites with diameters exceeding the maximum predicted diameter were also observed, and attributed to oval morphologies where the minor axis length was confined by the posts. Ring self-assembly was also observed around posts (Figs. 6, 7d), primarily with posts of 2 and $5 \mu\text{m}$ diameters. In fact, oval-shaped composites encircling two adjacent posts were observed in a number of cases for $2 \mu\text{m}$ post arrays (Fig. 6, upper left). Ring composites were observed assembled around $10 \mu\text{m}$ posts in very limited cases when the edge-to-edge spacing was $2 \mu\text{m}$ (Fig. 6, lower left).

DISCUSSION

Directed transport of microtubules has been achieved using combinations of chemical and physical

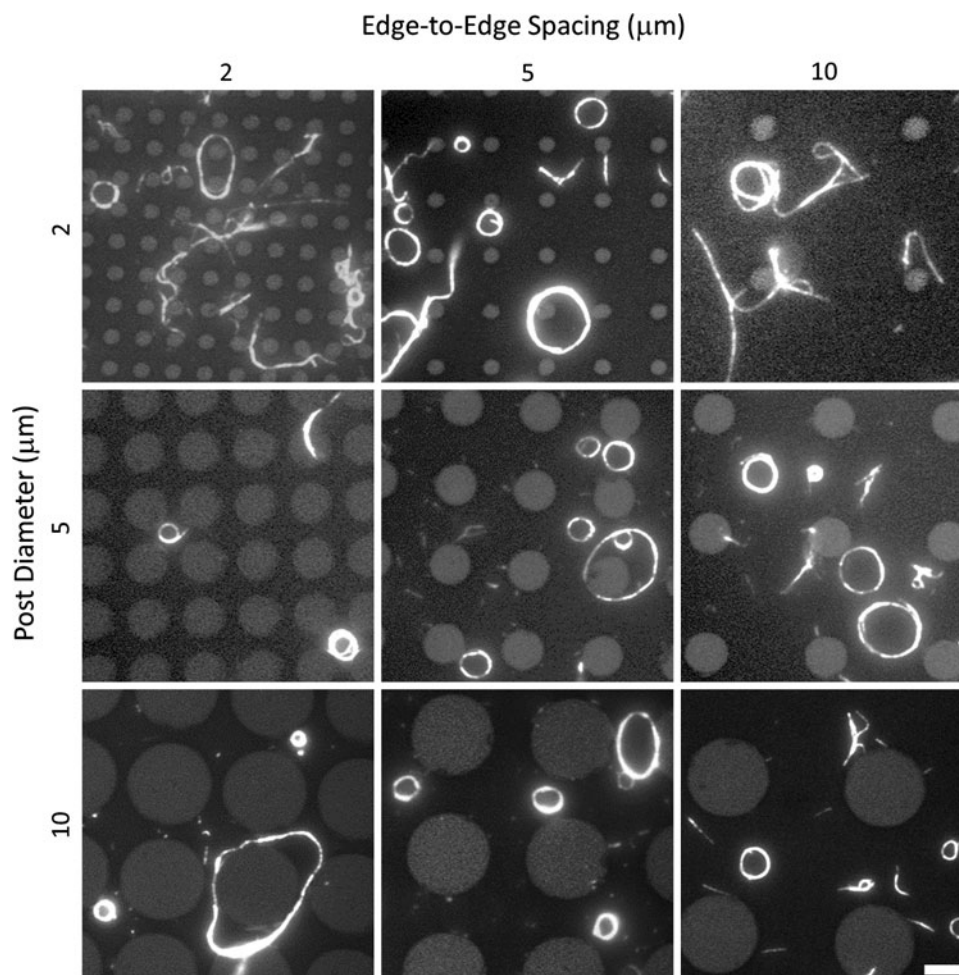


FIGURE 6. Fluorescence microscopy images showing ring composite self-assembly in square post arrays as a function of the varying diameters and edge-to-edge spacing distances. Scale bar = 5 μm .

surface patterns where chemical surface functionalization limits kinesin adhesion to specific regions, and physical barriers rectify and guide microtubule transport.^{4-6,13-15,28,29,37} A similar approach was applied in our study to understand the effects of confinement on the assembly of ring nanocomposites. Here, channels were microfabricated such that the tops and sidewalls were composed of gold and the channel bottoms were SiO_2 , which enabled selective functionalization of the tops and sidewalls through thiol chemistry. Confined self-assembly of ring composites was achieved when gold surfaces were functionalized with either PEG or cationic SAMs (Fig. 2). Lack of kinesin adsorption to the PEG-SAMs due to its anti-fouling nature enables selective adsorption of kinesin and subsequent self-assembly of ring composites only on the SiO_2 surface of the channel bottoms. Similarly, the cationic nature of the amine-terminated SAM either prevents motor adsorption or inactivates motors upon adsorption, preventing the assembly of ring composites on these

surfaces. Adsorption of microtubules, which possess an overall net negative charge,^{34,36} to cationic surfaces was also not observed and likely due to blocking by adsorbed casein. In contrast, surface selectivity was not observed with anionic SAMs as the anionic nature of both surfaces (i.e., SiO_2 and SAM-coated) equally supports adsorption of kinesin and the underlying casein layer (Figs. 2, 3). Detachment of mature ring composites from the anionic SAMs surfaces (Fig. 3), but not the SiO_2 surfaces, suggests that the kinesin interaction with the SAMs surface is not as strong. It is unclear whether ring detachment is a result of desorption of kinesin (with attached rings) from the SAM surface, unbinding of the ring composites from kinesin, or electrostatic repulsion of due to an increased charge density in the assembled rings. A lower surface density of active kinesin on the anionic SAMs, as compared to SiO_2 surfaces, also may explain the preferential detachment of ring structures SAM surfaces. Persistence of the ring composites in

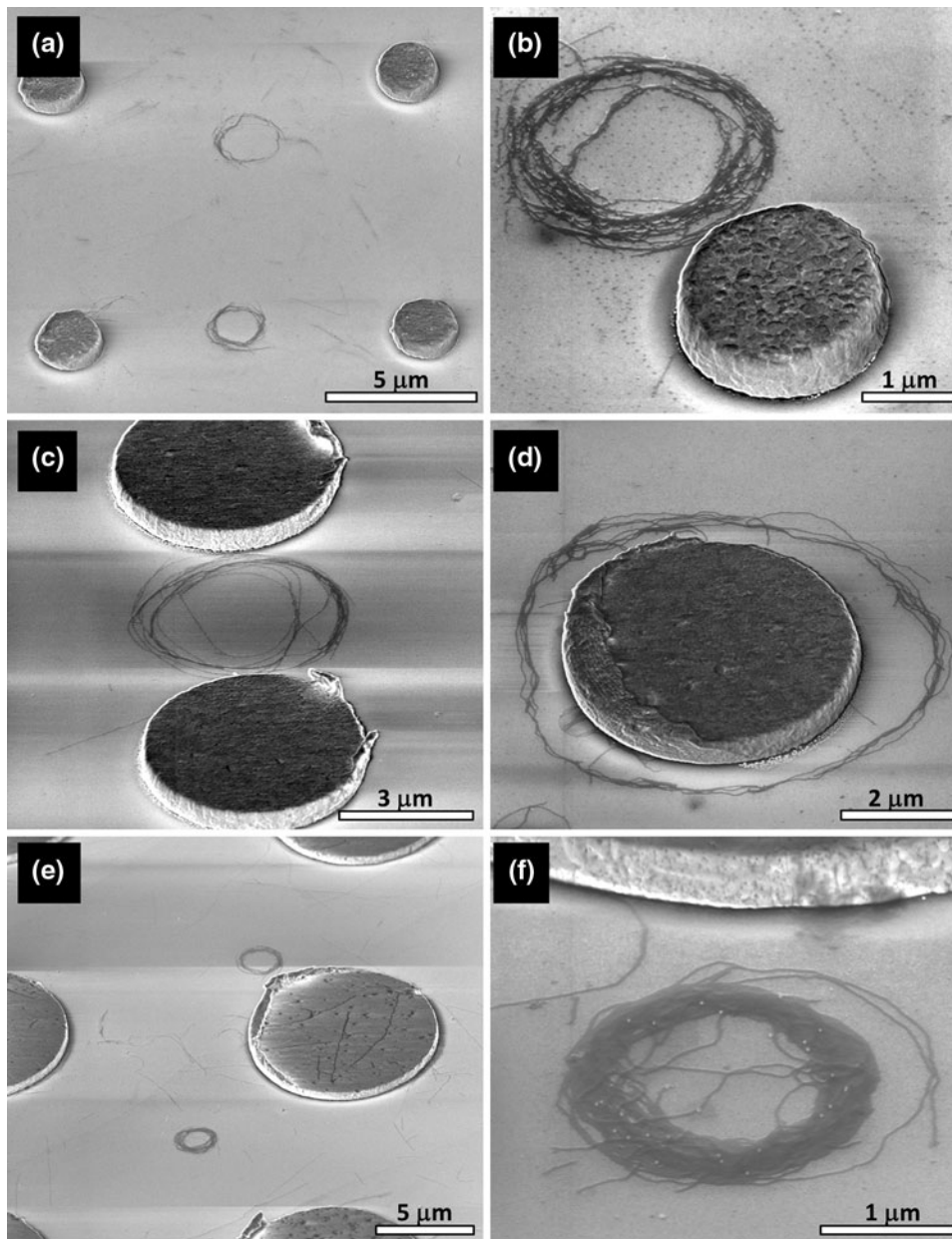


FIGURE 7. SEM images showing ring composite formation on surfaces of 2 μm (a, b), 5 μm (c, d) and 10 μm (e, f) gold posts, where the posts were functionalized with thiol-EG4 monolayer to prevent kinesin attachment to the posts.

solution, however, suggests that kinesin binding and transport are not required for the composites to maintain their structure and morphology. In all cases, rings that formed on anionic SAMS, in micro-fabricated channels, or in post arrays displayed preferential counter-clockwise rotation, as previously noted.^{20,23,24}

Interestingly, ring composites were able to form along the top edges of channels and capable of extending, unsupported, over the channel edge (Fig. 3). While the assembly of these rings was not directly observed, such cases may provide important insights into the ring

self-assembly process. We previously hypothesized that mechanical strain, developed through axially rotation of microtubule oligomers, initiates the self-assembly process and dictates the ring morphology.^{23,24} If one considers how ring assembly takes place at the top edges of channel walls, strain-induced curvature of QD-microtubule oligomers may enable it to bend back (i.e., make a U-turn) after it leaves the top surface of the channel, reattach to the kinesin surface, and complete the formation of the initial ring morphology. In the absence of strain energy and induced curvature, the microtubule oligomer should be considerably rigid,¹⁰ and thus con-

tinue forward translation over the channel edge until it eventually becomes completely detached from the surface. Similar observations have been previously noted as individual microtubules encounter a boundary between areas with and without surface-adsorbed kinesin motors.⁶ Thus, assembly at the edges of channels further suggests that mechanical strain intrinsic to oligomers may play a critical component to the self-assembly process.

Differences in the self-assembly of ring composites were observed due to confinement in microfluidic channels. While the average outer diameter of ring composites did not differ based on channel width, the observed average diameters of composites formed in the channels (i.e., 3.6 and 4.1 μm for 5 and 10 μm channels, respectively) were smaller than the previously reported average diameter of ring composites in the absence of confinement (i.e., 5.2 μm).^{23,24} Similarly, outer ring diameters up to 5.2 μm were observed in post arrays where the effects of confinement were minimal due to large interstitial spaces (Fig. 5). This effect may be attributed to how the composites assemble in the channel geometry, specifically where nucleation occurs with respect to the channel walls. Ring composites in which the nucleated center is coincident with the center of the channel are able to achieve the maximum diameter permissible based on confinement by both channel walls. This scenario, however, is statistically improbable based on the stochastic nature of the nucleation process. Therefore, the majority of ring composites will be confined by a single channel wall as radial growth of the ring occurs following nucleation. As a result, the majority of observed diameters will be significantly smaller than the channel width, and directly a function of the distance between the nucleation center and the closest channel wall. Moreover, a proportion of ring composites may assemble and reach a mature state without experiencing confinement by interacting with a channel wall. Differences in channel width did affect the distribution of ring composite diameters (Fig. 4), suggesting that physical confinement may be used to limit the assembly of composites with large diameters (i.e., exceeding the channel width). For example, ring composites with diameters exceeding 6 μm were observed in the 10 μm channels but not in the 5 μm channels. For both channel widths, oval-shaped composites were observed where the minor axis length was confined by the sidewalls of the channel and the major axis length exceeded the channel width. Similar oval-shaped, as well as irregularly shaped, composites have been observed on flat, planar surfaces,²³ and thus cannot be attributed to confinement of self-assembly within the channels. Overall these data suggest that confinement of self-assembly in channels may be an

effective strategy for reducing the average diameter and dispersity of ring composites.

Significant confinement effects on ring composite self-assembly were observed with the post arrays (Fig. 5) and primarily attributed to varying the spacing between posts. The maximum diameters of rings assembled within the interstitial spaces created by four posts in a square lattice were estimated to cover a range from 3.7 to 18.3 μm (Table 1) based on varying the diameters and edge-to-edge spacing distance. As with the channel geometry, diameter of the ring composites assembled in these patterns is primarily dependent on the distance of the nucleation center from the nearest post. The data suggest that spacing the posts at 2 μm edge-to-edge significantly reduces the average diameter of rings self-assembled in the post arrays (Fig. 5), which corresponds to interstitial spaces in which the maximum predicted ring diameter would be ≤ 7 μm . From these findings, confinement effects would have been expected with the 5- μm wide channels, and suggests that the confinement geometries (i.e., posts vs. channels) lead to differential effects on ring assembly. While post diameter has little effect on ring diameter, rings assembled around posts most commonly when the diameters was 2 or 5 μm ; only a few rings were found encircling 10 μm posts. In the future, changing the geometry from a square to hexagonal arrangement can provide an additional size range of interstitial spaces, as well as differential geometries, to further assess the effects of confinement of ring assembly. Moreover, tuning the diameter, spacing, and arrangement of posts in the arrays may permit the biased assembly of ring around posts as opposed to assembly in the interstitial spaces.

The effects of confinement on composite self-assembly provide important insights on the factors initiating and driving the self-assembly process. Two disparate mechanisms for initiating ring formation have been previously proposed: (1) mechanical strain build-up, and (2) surface pinning by inactive motors. As noted above, we have suggested that mechanical strain energy develops as coiled-coil and kinked domains form through axially rotation of microtubule oligomers.^{23,24} This energy enables the rigid microtubule oligomers to bend into ring structures capable of storing considerable amounts of elastic energy. As an alternate mechanism, Luria *et al.* suggest that surface pinning of microtubules by inactive motors and simultaneous crosslinking of microtubules initiates self-assembly of ring structures.²⁶ First, we will consider how rings can self-assemble at the edge of channels on the upper surface of the pattern, as shown in Fig. 3. Pinning of a microtubule at the edge of a channel by inactive motors should not lead to ring formation, particularly ones with large diameters, but

rather it should lead to a microtubule hanging over the edge of the channel with only the tip attached to the top surface. On the other hand, strain-induced curvature of microtubule oligomers could enable the rigid bundle to bend in a U-shape, allowing it to reattach to the upper surface and continue translation into the ring morphology. Because assembly of such rings was not directly observed, their formation at the edges of channels on the upper surface may have resulted from other mechanisms or phenomena (e.g., reattachment of floating rings at such locations). Additional experiments must be performed to verify the hypothesized mechanism presented above. The assembly of ring structures around posts in an array (Figs. 6, 7) also supports the mechanical strain hypothesis for initiating ring self-assembly. Assembly of rings in the interstitial spaces of post arrays could be initiated by surface pinning, but a mechanism by which the rings assemble around posts *via* surface pinning cannot be rationalized. In order to assemble a ring around a post, the leading tip of the microtubule or microtubule oligomer must traverse the perimeter of the post until it contacts and binds to itself, forming a completed ring structure. If the leading tip becomes pinned, a ring structure may form in the interstitial space, but would be unable to traverse the post's perimeter to form a ring encompassing the post. Conversely, one can easily conceptualize how mechanical strain and associated bending of microtubule oligomers could self-assemble around posts in an array. In such cases, the mechanical strain keeps the leading tip of the oligomer close to the post wall as it navigates the circumference, and, if long enough, crosslink to the tail of the oligomer. Thus, while surface pinning cannot be completely dismissed with respect to ring self-assembly, results from our experiments within confinement strongly support the critical role of mechanical strain energy, due to axial rotation of oligomers, in the self-assembly of ring nanocomposites.

CONCLUSIONS

Active transport *via* kinesin motors has been shown to provide a driving force for the assembly of non-equilibrium nanocomposite structures. Here, we have demonstrated and characterized the effects on confinement of ring composite assembly using microfabricated gold-SiO₂ substrates containing channels and posts, where the gold surfaces were rendered anti-fouling with thiol-SAMs. Confinement effects on the self-assembly of ring composites were observed in microfluidic channels, primarily with respect to the maximum ring diameter and distribution of ring diameters. With post arrays, rings with a significantly

smaller average diameter were self-assembled when the edge-to-edge spacing was 2 μm , compared against rings formed in arrays with 5 and 10 μm spacing. Together these data demonstrate that physical confinement by microfabricated structures may be used to control the average diameter and dispersity of ring composites. Observations including ring composite assembly along top edges of channels and around posts in the arrays confirm that mechanical strain formed by axial rotation of microtubule oligomers plays a central role in initiating the self-assembly process. Using top-down lithographic processing, we can now begin designing new surface patterns to confine kinesin-driven self-assembly with the goal of generating new composite morphologies.

ACKNOWLEDGMENTS

We thank Nathan Bouxsein and Marlene Bachand for their insight comments, suggestions, and feedback. We also thank Dr. Andrew Boal for intellectual input regarding gold-thiol functionalization to localize kinesin adsorption. This research was supported by the U.S. Department of Energy, Office of Basic Energy Sciences, Division of Materials Sciences and Engineering, Project KC0203010. Sandia National Laboratories is a multi-program laboratory operated by Sandia Corporation, a wholly owned subsidiary of Lockheed Martin Company, for the U.S. Department of Energy's National Nuclear Security Administration under contract DE-AC04-94AL85000.

REFERENCES

- ¹Bachand, G. D., S. B. Rivera, A. K. Boal, J. Gaudio, J. Liu, and B. C. Bunker. Assembly and transport of nanocrystal CdSe quantum dot nanocomposites using microtubules and kinesin motor proteins. *Nano Lett.* 4:817–821, 2004.
- ²Bachand, M., A. M. Trent, B. C. Bunker, and G. D. Bachand. Physical factors affecting kinesin-based transport of synthetic nanoparticle cargo. *J. Nanosci. Nanotechnol.* 5:718–722, 2005.
- ³Boal, A. K., G. D. Bachand, S. B. Rivera, and B. C. Bunker. Interactions between cargo-carrying biomolecular shuttles. *Nanotechnology* 17:349–354, 2006.
- ⁴Cheng, L. J., M. T. Kao, E. Meyhofer, and L. J. Guo. Highly efficient guiding of microtubule transport with imprinted CYTOP nanotracks. *Small* 1:409–414, 2005.
- ⁵Clemmens, J., H. Hess, J. Howard, and V. Vogel. Analysis of microtubule guidance in open microfabricated channels coated with the motor protein kinesin. *Langmuir* 19:1738–1744, 2003.
- ⁶Clemmens, J., H. Hess, R. Lipscomb, Y. Hanein, K. F. Bohringer, C. M. Matzke, G. D. Bachand, B. C. Bunker, and

- V. Vogel. Mechanisms of microtubule guiding on micro-fabricated kinesin-coated surfaces: chemical and topographic surface patterns. *Langmuir* 19:10967–10974, 2003.
- ⁷Coy, D. L., M. Wagenbach, and J. Howard. Kinesin takes one 8-nm step for each ATP that it hydrolyzes. *J. Biol. Chem.* 274:3667–3671, 1999.
- ⁸Dinu, C. Z., J. Opitz, W. Pompe, J. Howard, M. Mertig, and S. Diez. Parallel manipulation of bifunctional DNA molecules on structured surfaces using kinesin-driven microtubules. *Small* 2:1090–1098, 2006.
- ⁹Gittes, F., B. Mickey, J. Nettleton, and J. Howard. Flexural rigidity of microtubules and actin-filaments measured from thermal fluctuations in shape. *J. Cell. Biol.* 120:923–934, 1993.
- ¹⁰Guo, Y. X., Y. F. Liu, J. X. Tang, and J. M. Valles. Polymerization force driven buckling of microtubule bundles determines the wavelength of patterns formed in tubulin solutions. *Phys. Rev. Lett.* 98:198103, 2007.
- ¹¹Hess, H. Self-assembly driven by molecular motors. *Soft Matter* 2:669–677, 2006.
- ¹²Hess, H., J. Clemmens, C. Brunner, R. Doot, S. Luna, K. H. Ernst, and V. Vogel. Molecular self-assembly of “nanowires” and “nanospools” using active transport. *Nano Lett.* 5:629–633, 2005.
- ¹³Hess, H., J. Clemmens, C. Matzke, G. Bachand, B. Bunker, and V. Vogel. Ratchet patterns sort molecular shuttles. *Appl. Phys. A* 75:309–313, 2002.
- ¹⁴Hess, H., C. M. Matzke, R. Doot, J. Clemmens, G. D. Bachand, B. C. Bunker, and V. Vogel. Molecular shuttles operating undercover: a new photolithographic approach for the fabrication of structured surfaces supporting directed motility. *Nano Lett.* 3:1651–1655, 2003.
- ¹⁵Hiratsuka, Y., T. Tada, K. Oiwa, T. Kanayama, and T. Q. P. Uyeda. Controlling the direction of kinesin-driven microtubule movements along microlithographic tracks. *Biophys. J.* 81:1555–1561, 2001.
- ¹⁶Hutchins, B. M., M. Platt, W. O. Hancock, and M. E. Williams. Motility of CoFe_2O_4 nanoparticle-labelled microtubules in magnetic fields. *Micro Nano Lett.* 1:47–52, 2006.
- ¹⁷Hutchins, B. M., M. Platt, W. O. Hancock, and M. E. Williams. Directing transport of CoFe_2O_4 -functionalized microtubules with magnetic fields. *Small* 3:126–131, 2007.
- ¹⁸Jia, L. L., S. G. Moorjani, T. N. Jackson, and W. O. Hancock. Microscale transport and sorting by kinesin molecular motors. *Biomed. Microdevices* 6:67–74, 2004.
- ¹⁹Kawamura, R., A. Kakugo, Y. Osada, and J. P. Gong. Microtubule bundle formation driven by ATP: the effect of concentrations of kinesin, streptavidin and microtubules. *Nanotechnology* 21:145603–145614, 2010.
- ²⁰Kawamura, R., A. Kakugo, K. Shikinaka, Y. Osada, and J. P. Gong. Ring-shaped assembly of microtubules shows preferential counterclockwise motion. *Biomacromolecules* 9:2277–2282, 2008.
- ²¹Kawamura, R., A. Kakugo, K. Shikinaka, Y. Osada, and J. P. Gong. Formation of motile assembly of microtubules driven by kinesins. *Smart Mater. Struct.* 20:129901, 2011.
- ²²Kim, T., L. J. Cheng, M. T. Kao, E. F. Hasselbrink, L. J. Guo, and E. Meyhofer. Biomolecular motor-driven molecular sorter. *Lab. Chip* 9:1282–1285, 2009.
- ²³Liu, H., and G. D. Bachand. Understanding energy dissipation and thermodynamics in biomotor-driven nanocomposite assemblies. *Soft Matter* 7:3087–3091, 2011.
- ²⁴Liu, H. Q., E. D. Spoerke, M. Bachand, S. J. Koch, B. C. Bunker, and G. D. Bachand. Biomolecular motor-powered self-assembly of dissipative nanocomposite rings. *Adv. Mater.* 20:4476–4481, 2008.
- ²⁵Love, J. C., L. A. Estroff, J. K. Kriebel, R. G. Nuzzo, and G. M. Whitesides. Self-assembled monolayers of thiolates on metals as a form of nanotechnology. *Chem. Rev.* 105:1103–1169, 2005.
- ²⁶Luria, I., J. Crenshaw, M. Downs, A. Agarwal, S. B. Seshadri, J. Gonzales, O. Idan, J. Kamcev, P. Katira, S. Pandey, T. Nitta, S. R. Phillpot, and H. Hess. Microtubule nanospool formation by active self-assembly is not initiated by thermal activation. *Soft Matter* 7:3108–3115, 2011.
- ²⁷Martin, B. D., C. M. Soto, A. S. Blum, K. E. Sapsford, J. L. Whitley, J. E. Johnson, A. Chatterji, and B. R. Ratna. An engineered virus as a bright fluorescent tag and scaffold for cargo proteins—capture and transport by gliding microtubules. *J. Nanosci. Nanotechnol.* 6:2451–2460, 2006.
- ²⁸Moorjani, S. G., L. Jia, T. N. Jackson, and W. O. Hancock. Lithographically patterned channels spatially segregate kinesin motor activity and effectively guide microtubule movements. *Nano Lett.* 3:633–637, 2003.
- ²⁹Nitta, T., A. Tanahashi, Y. Obara, M. Hirano, M. Razumova, M. Regnier, and H. Hess. Comparing guiding track requirements for myosin- and kinesin-powered molecular shuttles. *Nano Lett.* 8:2305–2309, 2008.
- ³⁰Pampaloni, F., G. Lattanzi, A. Jonas, T. Surrey, E. Frey, and E. L. Florin. Thermal fluctuations of grafted microtubules provide evidence of a length-dependent persistence length. *Proc. Natl. Acad. Sci. USA* 103:10248–10253, 2006.
- ³¹Papra, A., N. Gadegaard, and N. B. Larsen. Characterization of ultrathin poly(ethylene glycol) monolayers on silicon substrates. *Langmuir* 17:1457–1460, 2001.
- ³²Pinot, M., F. Chesnel, J. Z. Kubiak, I. Arnal, F. J. Nedelec, and Z. Gueroui. Effects of confinement on the self-organization of microtubules and motors. *Curr. Biol.* 19:954–960, 2009.
- ³³Ramanathan, M., S. M. Kilbey, Q. M. Ji, J. P. Hill, and K. Ariga. Materials self-assembly and fabrication in confined spaces. *J. Mater. Chem.* 22:10389–10405, 2012.
- ³⁴Safinya, C. R., D. J. Needleman, M. A. Ojeda-Lopez, U. Raviv, H. P. Miller, and L. Wilson. Higher-order assembly of microtubules by counterions: from hexagonal bundles to living necklaces. *Proc. Natl. Acad. Sci. USA* 101:16099–16103, 2004.
- ³⁵Service, R. F. How far can we push chemical self-assembly. *Science* 309:95, 2005.
- ³⁶Stebbing, H., and C. Hunt. The nature of the clear zone around microtubules. *Cell Tissue Res.* 227:609–617, 1982.
- ³⁷van den Heuvel, M. G. L., C. T. Butcher, R. M. M. Smeets, S. Diez, and C. Dekker. High rectifying efficiencies of microtubule motility on kinesin-coated gold nanostructures. *Nano Lett.* 5:1117–1122, 2005.
- ³⁸van den Heuvel, M. G. L., M. P. De Graaff, and C. Dekker. Molecular sorting by electrical steering of microtubules in kinesin-coated channels. *Science* 312:910–914, 2006.
- ³⁹Whitesides, G. M., and B. Grzybowski. Self-assembly at all scales. *Science* 295:2418–2421, 2002.
- ⁴⁰Whitesides, G. M., J. P. Mathias, and C. T. Seto. Molecular self-assembly and nanochemistry—a chemical strategy for the synthesis of nanostructures. *Science* 254:1312–1319, 1991.